VSP

Advanced Composite Materials 18 (2009) 135–152

ADVANCED COMPOSITE MATERIALS
www.brill.nl/acm

Similarity Relations of Resin Flow in Resin Transfer Molding Process

Moon-Kwang Um [a,*], **Joon-Hyung Byun** [a] **and Isaac M. Daniel** [b]

[a] Korea Institute of Materials Science, Composite Materials Group, 531 Changwondaero, Changwon, Kyeongnam, 641-831, South Korea

[b] Departments of Civil and Environmental Engineering and Mechanical Engineering, Center for Intelligent Processing of Composites, Northwestern University, Evanston, IL 60208-3020, USA

Received 18 December 2007; accepted 9 May 2008

Abstract

Liquid molding processes, such as resin transfer molding, involve resin flow through a porous medium inside a mold cavity. Numerical analysis of resin flow and mold filling is a very useful means for optimization of the manufacturing process. However, the numerical analysis is quite time consuming and requires a great deal of effort, since a separate numerical calculation is needed for every set of material properties, part size and injection conditions. The efforts can be appreciably reduced if similarity solutions are used instead of repeated numerical calculations. In this study, the similarity relations for pressure, resin velocity and flow front propagation are proposed to correlate another desired case from the already obtained numerical result. In other words, the model gives a correlation of flow induced variables between two different cases. The model was verified by comparing results obtained by the similarity relation and by independent numerical simulation.

Keywords

Resin transfer molding, similarity relations of flow field, pressure relation, velocity relation, relation of flow front advancement time

1. Introduction

In the liquid molding process of composites, numerical analysis of mold filling is a useful and necessary means of process optimization, such as determination of gate/vent locations and their opening–closing sequence, control of injection pressure and flow rate [1–4]. The analysis also helps in the selection of a suitable material system. For simple geometries, analytic solutions can be used to estimate the mold filling pattern [5, 6]. However, in many cases of realistic and complex geome-

* To whom correspondence should be addressed. E-mail: umk1693@kims.re.kr
Edited by KPCM

 DOI:10.1163/156855109X428745

tries, numerical methods have been employed to obtain accurate solutions. Various numerical schemes, such as the finite difference method [7, 8], the boundary element method [9, 10], and the finite element method [11–22], have been adopted and tested. At present, a control volume based finite element method (CVFEM) is a widely accepted method due to its relative ease of implementation and effectiveness in treating the moving flow front without mesh regeneration.

In general, a great deal of effort is necessary to perform a numerical analysis as it requires mesh generation, input data preparation, post processing of the result, etc. However, the effort is appreciably reduced by using similarity solutions, which obviate the need for repeated simulations. In this paper, similarity relations of variables induced in resin flow are proposed to obtain multiple results for many cases based on data from only one numerical analysis.

2. Similarity Relations

The conservation of momentum for resin flow through a fiber preform is described by the well-known Darcy law [23]. Darcy's law is a kind of simplified form of the Navier–Stokes equation for resin flow through porous media. The flow through porous media is assumed to be a low Reynolds number flow in which the inertia force is negligible and the pressure force balances the viscous force.

$$\bar{u}_{\mathrm{D}} = -\frac{[K]}{\mu}\nabla P, \tag{1}$$

where $\bar{u}_{\mathrm{D}}$ is a Darcian velocity, $[K]$ the permeability matrix of the reinforcement, P pressure, ∇P its gradient, and μ the resin viscosity. Here, the resin is assumed to be an incompressible Newtonian liquid. Actually, the Darcian velocity is an imaginary velocity and the real velocity that we observe in mold filling is an apparent or pore velocity ($\bar{u}_{\mathrm{P}}$) defined as

$$\bar{u}_{\mathrm{P}} = \frac{\bar{u}_{\mathrm{D}}}{\varepsilon} = -\frac{[K]}{\varepsilon\mu}\nabla P, \tag{2}$$

where $\varepsilon = 1 - V_f$ (porosity), V_f = fiber volume ratio.

The governing equation of resin flow is obtained by substituting the apparent velocity into the mass conservation equation

$$\nabla \cdot \bar{u}_{\mathrm{P}} = \nabla \cdot \left(-\frac{[K]}{\varepsilon\mu}\nabla P \right) = 0. \tag{3}$$

If the partial differential equation is linear and homogeneous, the solution obtained for the given material properties, the part geometry and the boundary conditions, is also a solution for the case where all these parameters are changed. The existence of a similarity solution is deduced from the fact that the governing equation (3) is linear and homogeneous. Also, the analogy of flow front shapes shown in the cases where the properties and the conditions are different guarantees the existence of similarity solutions. The boundary conditions for solving the pressure field are

summarized as follows

$$\text{Injection Gate: } P = P_i(t) \tag{4}$$

$$\text{Mold Wall: } \frac{\partial P}{\partial n} = 0 \tag{5}$$

$$\text{Flow Front: } P = 0, \tag{6}$$

where $P_i(t)$ is the pressure at the gate and n denotes the direction normal to the mold wall.

When the flow is assumed to be quasi-steady, the pressure field is obtained by solving the governing differential equation (3) with the given boundary conditions (equations (4)–(6)). The solution technique can be either analytical or numerical. For example, the solution of the pressure field can be determined through the variational or weak formulation of (3) and application of the boundary conditions,

$$\iiint_R w\nabla \cdot \bar{u}_P \, \mathrm{d}V = \iiint_R w\nabla \cdot \left(\frac{[K]}{\varepsilon\mu}\nabla P\right) \mathrm{d}V = 0, \tag{7}$$

where w is a weight function, R the region filled with resin and V the volume. With the aid of the pressure field obtained by (7), the velocity field at that instant is calculated from (2). Then, the flow front is advanced with the resin velocity and the same procedure is repeated for the newly filled region. To derive similarity relations, additional assumptions are made as follows:

- In general, the viscosity changes as chemical reaction progresses (Fig. 1). The resin is premixed and then injected into the mold. The mixed resin experiences the same temperature history throughout the process. Therefore, the viscosity at the specific instant of mold fill is uniform throughout the impregnated region.
- The drag force induced by the flow does not cause distortion of the preform; thus, the permeability does not change during the flow.

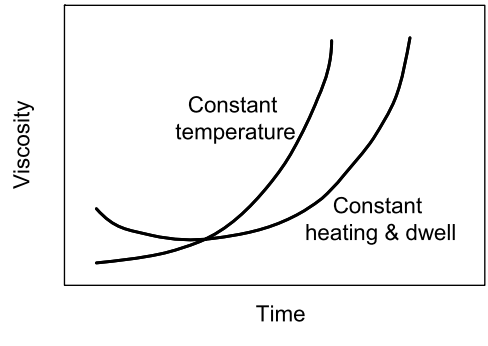

Figure 1. Variation of resin viscosity with time due to chemical reaction.

To find the similarity relations, two problems are examined: an original or reference problem and a sample one with different material and geometric properties and process conditions.

2.1. Similarities in Pressure and Its Gradient Field

As a first step in mold filling analysis the pressure field must be determined in the impregnated region. The material properties, part geometry and injection pressure for driving the model are defined in Table 1 and Fig. 2. The injection pressure and boundary conditions for the pressure field can be selectively defined according to the process requirements (Fig. 3). When the resin is injected through multiple gates, the ratios of injection pressures at the gates in the original problem should be equal

Table 1.
Material properties, part geometry and injection pressure

		Original	Sample
Reinforcement	Permeability, $[K]$ Porosity, ε	$[K]_{o,i} \quad (1 \leqslant i \leqslant n)$ $\varepsilon_{o,i} \quad (1 \leqslant i \leqslant n)$	$[K]_{s,i} = a_K[K]_{o,i} \quad (1 \leqslant i \leqslant n)$ $\varepsilon_{s,i} = a_\varepsilon \varepsilon_{o,i} \quad (1 \leqslant i \leqslant n)$
Resin	Viscosity, μ	$\mu_o(t)$	$\mu_s(t)$
Part shape, $\mathbf{X}$ ($\mathbf{X}$: position vector)		$\mathbf{X}_{o,i} \quad (1 \leqslant i \leqslant n)$ (n: number of reinforcement)	$\mathbf{X}_s = a_L \mathbf{X}_o$ $\mathbf{X}_s = (x^*, y^*, z^*)$ $\mathbf{X}_o = (x, y, z)$
Injection pressure, P		$P_o(t) = P_{o,k}(t)$ $(k = 1, \ldots, l)$ (l: number of injection port)	$P_s(t) = P_{s,k}(t) \quad (k = 1, \ldots, l)$

t: time, subscript 'o' and 's': the original and the sample.
a_ε, a_K, a_L: scale factors between the original and the sample.

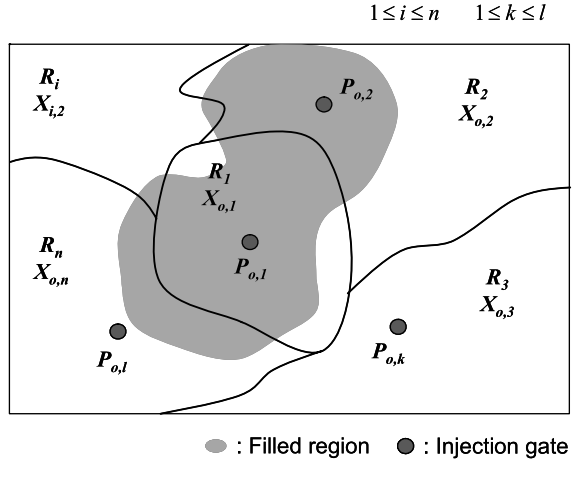

Figure 2. Definitions of properties and variables for deriving similarity relations.

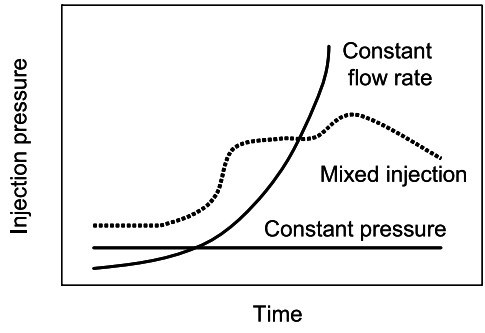

Figure 3. Types of resin injection.

to those in the sample problem to maintain the analogy of flow front shape between the two cases. This is an important requirement for the existence of a similarity solution for multiple-gate injection.

$$\frac{P_{\mathrm{o},k}(t)}{P_{\mathrm{o},1}(t)} = \frac{P_{\mathrm{s},k}(t)}{P_{\mathrm{s},1}(t)} \quad (2 \leqslant k \leqslant l), \tag{8}$$

where $P_{\mathrm{o},1}(t)$ and $P_{\mathrm{s},1}(t)$ are the first gates in the original and sample cases where the resin is injected into the mold. In the case of sequentially opened multiple gates, the open time at each gate should also be adjusted in the sample problem and it will be described in detail in the 'time scale transformation' section below. In the case of a single gate, the gate open time and the ratio of pressures are not required for development of the model.

Applying equation (7) to m components of reinforcement filled with resin at a specific instant in the original problem (Fig. 2), we obtain

$$\begin{aligned} &\iiint_{R_1} w\nabla\cdot\left(\frac{[K]_{\mathrm{o},1}}{\varepsilon_{\mathrm{o},1}\mu_{\mathrm{o}}(t)}\nabla P\right)\mathrm{d}V + \cdots + \iiint_{R_m} w\nabla\cdot\left(\frac{[K]_{\mathrm{o},m}}{\varepsilon_{\mathrm{o},m}\mu_{\mathrm{o}}(t)}\nabla P\right)\mathrm{d}V \\ &= \frac{1}{\mu_{\mathrm{o}}(t)}\sum_{j=1}^{m}\left\{\iiint_{R_j} w\nabla\cdot\left(\frac{[K]_{\mathrm{o},j}}{\varepsilon_{\mathrm{o},j}}\nabla P\right)\mathrm{d}V\right\} = 0 \quad (1 \leqslant m \leqslant n), \end{aligned} \tag{9}$$

where R_j is the jth component of reinforcement in the impregnated region. Here, we assume the solution of pressure field at the jth reinforcement component as

$$\text{Solution of pressure field } = [P(\mathbf{X}_{\mathrm{o},j}, t_{\mathrm{o}})]_{\mathrm{sol}} \quad 1 \leqslant j \leqslant m, \tag{10}$$

where $\mathbf{X}_{\mathrm{o},j}$ is the position vector defining the jth reinforcement and t_{o} the time scale in the original problem.

Applying equation (7) to the filled region in the sample case by analogy with the original, we obtain

$$\frac{1}{\mu_{\mathrm{s}}(t)}\sum_{j=1}^{m}\left\{\iiint_{R_j^*} w\nabla\cdot\left(\frac{[K]_{\mathrm{s},j}}{\varepsilon_{\mathrm{s},j}}\nabla P\right)\mathrm{d}V^*\right\} = 0 \quad (1 \leqslant m \leqslant n), \tag{11}$$

where R_j^* is the jth reinforcement component of the sample case and equation (1) 1 is a volume integral in the sample. The above integral can be transformed into that of the original case by introducing the Jacobian cubic (a_L^3) and the scale factors a_K and a_ε accounting for the permeability and porosity effects on the transformation.

$$\frac{a_K a_L^3}{a_\varepsilon}\frac{1}{\mu_s(t)}\sum_{j=1}^{m}\left\{\iiint_{R_j} w\nabla\cdot\left(\frac{[K]_{o,j}}{\varepsilon_{o,j}}\nabla P\right)\mathrm{d}V\right\}=0 \quad (1\leqslant m\leqslant n). \tag{12}$$

The integral part of (12) is the same as that of (9). Therefore, based on the linearity and homogeneity of the governing equation, the solution of (12) is determined by the ratio of injection boundary conditions between the two cases. This ratio can be described by the pressure at the first gates, $P_{o,1}(t_o)$ and $P_{s,1}(t_s)$, which are representative of the two cases (equation (8)). The relation between t_o and t_s is explained below in the 'time scale transformation' section. The solution of (12), the pressure field, and its gradient are described as follows by considering equation (10) and Table 1.

$$[P(\mathbf{X}_{s,j},t_s)]_{sol}=\frac{P_{s,1}(t_s)}{P_{o,1}(t_o)}[P(\mathbf{X}_{o,j},t_o)]_{sol} \quad 1\leqslant j\leqslant m, \tag{13}$$

$$[\nabla P(\mathbf{X}_{s,j},t_s)]_{sol}=\frac{1}{a_L}\frac{P_{s,1}(t_s)}{P_{o,1}(t_o)}[\nabla P(\mathbf{X}_{o,j},t_o)]_{sol} \quad 1\leqslant j\leqslant m, \tag{14}$$

where $\mathbf{X}_{s,j}$ is a position vector of the jth reinforcement component in the sample problem. Finally, (13) and (14) represent similarity relations of pressure and its gradient between the original and the sample cases at a specific instant of mold fill. It is known from (13) and (14) that the similarities of pressure and its gradient are dependent on the injection pressure ratio and the part size scale factor.

2.2. Similarity in Resin Flow Velocity

Resin flow is induced by the pressure gradient developed in the flow field and the gradient determines the resin penetrating velocity through the porous medium. Therefore, the obtained pressure gradient is used to determine resin velocity (equation (2)). The apparent resin velocity in the flow region of the original case can be rewritten as

$$\bar{u}_p(\mathbf{X}_{o,j},t_o)=-\frac{[K]_{o,j}}{\mu_o(t_o)\varepsilon_{o,j}}[\nabla P(\mathbf{X}_{o,j},t_o)]_{sol} \quad (1\leqslant j\leqslant m). \tag{15}$$

For the flow front shape of the sample which has an analogy with that of the original, resin velocity is expressed as follows with the aid of the scaling factors of material property, viscosity, injection pressure and velocity of the original problem.

$$\begin{aligned}\bar{u}_p(\mathbf{X}_{s,j},t_s)&=-\frac{[K]_{s,j}}{\mu_s(t_s)\varepsilon_{s,j}}[\nabla P(\mathbf{X}_{s,j},t_s)]_{sol,j}\\&=\frac{a_K}{a_\varepsilon a_L}\frac{\mu_o(t_o)}{\mu_s(t_s)}\frac{P_s(t_s)}{P_o(t_o)}\bar{u}_p(\mathbf{X}_{o,j},t_o) \quad (1\leqslant j\leqslant m).\end{aligned} \tag{16}$$

Equation (16) is the final form of resin velocity similarity between the original and the sample problems at a specific instant of mold fill. It is shown from (16) that the similarity of resin velocities depends upon all the material properties, part size and injection boundary conditions.

2.3. Similarity in Flow Front Time Scale Transformation

It is deduced from the similarity of flow front shapes that there is only a change of time scale between corresponding points on the flow fronts. The time transformation is formulated as follows. As a starting point, the similarity of resin velocity, equation (16), is resolved into displacement (S) and time expressed as

$$\frac{\mu_{\mathrm{o}}(t_{\mathrm{o}})}{\mu_{\mathrm{s}}(t_{\mathrm{s}})}\frac{P_{\mathrm{s},1}(t_{\mathrm{s}})}{P_{\mathrm{o},1}(t_{\mathrm{o}})}\frac{\mathrm{d}t_{\mathrm{s}}}{\mathrm{d}t_{\mathrm{o}}} = \frac{a_\varepsilon a_{\mathrm{L}}}{a_{\mathrm{K}}}\frac{\mathrm{d}S_{\mathrm{s},j}}{\mathrm{d}S_{\mathrm{o},j}} \quad (1 \leqslant j \leqslant m). \tag{17}$$

The flow fronts for the two cases at a specific time match exactly by applying the part geometrical scale factor (a_{L}) to the displacement because the flow front is a time integral of the displacement.

$$S_{\mathrm{s},j} = a_{\mathrm{L}} S_{\mathrm{o},j} \quad (1 \leqslant j \leqslant m). \tag{18}$$

By replacing (17) with (18) and integrating it with respect to time, the transformation rule gives

$$\int_0^{t_{\mathrm{s}}} \frac{P_{\mathrm{s}}(t)}{\mu_{\mathrm{s}}(t)}\,\mathrm{d}t = \frac{a_\varepsilon a_{\mathrm{L}}^2}{a_{\mathrm{K}}} \cdot \int_0^{t_{\mathrm{o}}} \frac{P_{\mathrm{o}}(t)}{\mu_{\mathrm{o}}(t)}\,\mathrm{d}t. \tag{19}$$

The relation between time scales t_{o} and t_{s} in (13)–(15) is determined by (19). This equation is the time scale transformation for flow fronts between the original and the sample case. It is known from (19) that the similarity in time scales is also dependent on all the material properties, part size and injection boundary conditions.

3. Numerical Simulation of Flow Field

Resin flow can be predicted by means of experimental, analytical or numerical methods. The most powerful method for solving a real problem is numerical analysis. Therefore, a numerical scheme was applied to verify the suggested similarity relations. A numerical formulation was performed for a three-dimensional shell structure, which is locally a two-dimensional case. Of course, the similarity model is valid for mold filling of fully three-dimensional structures.

All parameters and properties were averaged through the thickness direction, as the shell structure can be regarded as two-dimensional locally. The pressure field was formulated using the Galerkin finite element scheme [24]. The formulation starts with the discretization of the calculation domain into a finite number of triangular shell elements (Fig. 4). The weak formulation of the governing equation

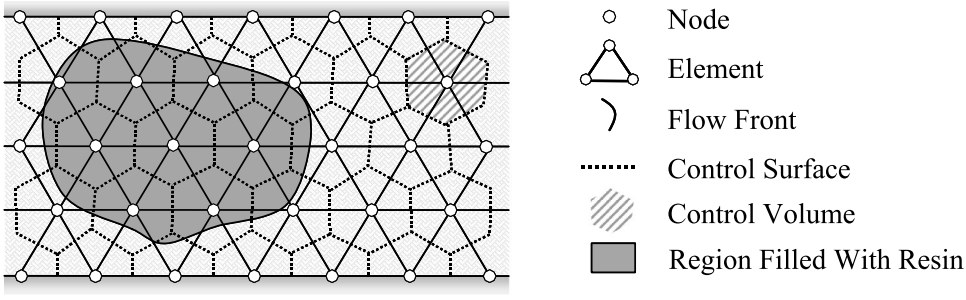

Figure 4. Definitions used in numerical formulations.

can be obtained by multiplying by a weight function w and integrating it over the domain.

$$\int_A w(\nabla \cdot \bar{u}_P)\,\mathrm{d}A = 0, \tag{20}$$

where A means an area or a calculation domain filled with resin in the locally two-dimensional plane and $\bar{u}_P$ the apparent resin velocity. Now, we define the flow conductance $S(=[K]/\mu\varepsilon)$ in (3) to simplify the derivation. Equation (20) can be rearranged using the flow conductance, the integration-by-parts formula and the divergence theorem as follows

$$\int_A S(\nabla w \cdot \nabla P)\,\mathrm{d}A = \int_\Gamma S(\bar{n} \cdot \nabla P) w\,\mathrm{d}\Gamma = \int_\Gamma S\frac{\partial P}{\partial n} w\,\mathrm{d}\Gamma, \tag{21}$$

where Γ is the calculation boundary, $\bar{n}$ a unit vector normal to the calculation boundary and $\frac{\partial P}{\partial n}$ the pressure gradient normal to the boundary.

The volumetric flux $(-S\frac{\partial P}{\partial n})$ on the right-hand side of (21) can be modified by using the natural boundary condition

$$-S\frac{\partial P}{\partial n} = s(P - \widehat{P}), \tag{22}$$

where s, $\widehat{P}$ are the coefficients imposed on the real pressure field boundary. This is a type of price paid for the ease of formulation. Since (21) is valid for the entire calculation domain, it can be applied to an element A_e as well

$$\int_{A_e} S_e(\nabla w \cdot \nabla P)\,\mathrm{d}A_e + \int_{\Gamma_e} s_e P w\,\mathrm{d}\Gamma_e = \int_{\Gamma_e} s_e \widehat{P} w\,\mathrm{d}\Gamma_e, \tag{23}$$

where subscript e denotes the element. Approximating the state variable P and the weight function w with the same shape function,

$$P^e(x, y) = \sum_{j=1}^{N_e} P_j^e \psi_j^e(x, y), \qquad w^e(x, y) = \sum_{j=1}^{N_e} w_j^e \psi_j^e(x, y), \tag{24}$$

where N_e is the number of nodes in the element, P_j^e the pressure value at the j node in the e element, ψ_j^e a local shape function of the element, w_j^e a weight constant at

the j node in the e element, and $P^{\mathrm{e}}(x, y)$ and $w^{\mathrm{e}}(x, y)$ a state variable and a weight in the element, respectively. The equation generated by substituting (24) into (23) should be satisfied for any weight constant w_j^{e}. Therefore, the stiffness matrix and the load vector for the element are

$$\sum_{j=1}^{N_{\mathrm{e}}} A_{ij}^{\mathrm{e}} P_j^{\mathrm{e}} = B_i^{\mathrm{e}} \quad i = 1, 2, \ldots, N_{\mathrm{e}}, \tag{25}$$

where

$$A_{ij}^{\mathrm{e}} = \int_{A_{\mathrm{e}}} S_{\mathrm{e}} \left(\frac{\partial \psi_i^{\mathrm{e}}}{\partial x} \frac{\partial \psi_j^{\mathrm{e}}}{\partial x} + \frac{\partial \psi_i^{\mathrm{e}}}{\partial y} \frac{\partial \psi_j^{\mathrm{e}}}{\partial y} \right) \mathrm{d}A_{\mathrm{e}} + \int_{\Gamma_{\mathrm{e}}} s_{\mathrm{e}} \psi_i^{\mathrm{e}} \psi_j^{\mathrm{e}} \, \mathrm{d}\Gamma_{\mathrm{e}}, \tag{26}$$

$$B_i^{\mathrm{e}} = \int_{A_{\mathrm{e}}} \psi_i^{\mathrm{e}} \, \mathrm{d}A_{\mathrm{e}} + \int_{\Gamma_{\mathrm{e}}} s_{\mathrm{e}} \widehat{P} \psi_i^{\mathrm{e}} \, \mathrm{d}\Gamma_{\mathrm{e}}. \tag{27}$$

In fact, the boundary integral terms of (26) and (27) vanish when the elements exist inside a real mold space due to the conservation of volume flux. They have their own effects when the element boundary coincides with the real mold boundary. The stiffness matrix and the load vector obtained from the elements are added up to form the global stiffness matrix and the load vector. Finally, the pressure field is determined by solving the system of equations made up of the global stiffness matrix and the load vector. The resin velocity at a specific time is calculated from the pressure gradient (equation (3)). The velocity at the flow front is used to advance the resin front at each time step.

The flow front advancement scheme is described as follows. The region filled with resin or the calculation domain changes as the flow front proceeds. This means that there is a moving boundary and it causes the main difficulty in the numerical simulation. The proper description of the domain filled with resin is very important because it plays a crucial role in the accurate prediction of the flow front and the related physical parameters. In general, there can be two choices for a grid system, a moving grid or a fixed grid. In the moving grid system, the calculation domain can be precisely described by regenerating new grids at the specific mold fill time. But if the domain is very complex, the discretization itself causes another difficulty. On the other hand, in the fixed grid system, the grids generated at the beginning are used throughout the calculation. This greatly relieves the burden of node regeneration and this is why the fixed grid system is widely used and was selected for this study.

Polyhedral control volumes in the domain are defined by connecting the centroids of the elements and the midpoints of the element sides (Fig. 4). The boundary of each polyhedron constitutes the control surface of the corresponding control volume and mass transfer takes place through this surface. Each control volume element is represented by a nodal point located at the center of the control volume element. The control volume elements are classified into three categories according to the volume fraction of resin infiltration (f_{r}).

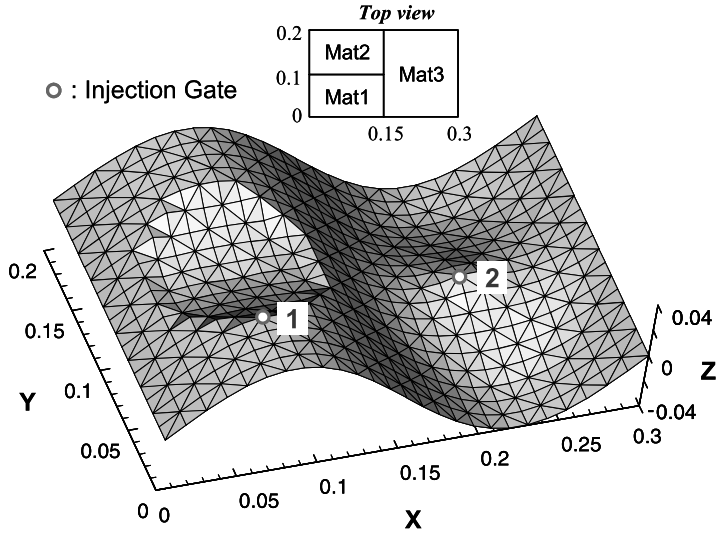

Figure 5. Geometry and mesh for numerical simulation in the original case.

– Fully filled region: $f_r = 1$.

– Empty region: $f_r = 0$.

– Flow front region: $0 < f_r < 1$.

The fill ratio f_r of each control volume element is calculated and updated during mold filling. When the fill ratio becomes unity, the nodal point becomes a part of the fully filled region.

The participation of the flow front nodes into the calculation domain is determined according to their fill fractions. The control volumes whose fill fractions lie between 0 and 1 are taken as the flow front control volumes. The time when the filled fraction f_r is 0.5 is recorded. The meaning of $f_r = 0.5$ is that the flow front just passes through the particular nodal point, namely, the centroid of the control volume. The fill fraction value of 0.5 is statistically found to be the best value to represent the flow front as it passes through the center of the control volume and is widely accepted in most moving boundary problems using fixed grids. The recorded fill times are then interpolated to obtain the flow front lines. These lines become smoother and closer to the real flow fronts as the node density increases.

The numerical scheme was verified by comparing the calculated and predicted complete fill times for the injection condition of constant flow rate in the original problem. Resin was injected through Gate 1 (Fig. 5). The calculated fill time for the part volume of 2.064×10^{-4} m^3, preform porosity of 0.5 and flow rate of 1.0×10^{-5} m^3/s is 10.32 s, whereas that determined by numerical simulation is 10.30 s for an error of approximately 0.20%.

Table 2.
Material properties used in the original problem

Reinforcement	Permeability, $[K]$	Mat 1	$[K]_{o,1} = \begin{bmatrix} 10\times10^{-10} & 0 \\ 0 & 8\times10^{-10} \end{bmatrix} \text{m}^2$,	$\theta = 135°$
		Mat 2	$[K]_{o,2} = \begin{bmatrix} 6\times10^{-10} & 0 \\ 0 & 4\times10^{-10} \end{bmatrix} \text{m}^2$,	$\theta = 0°$
		Mat 3	$[K]_{o,3} = \begin{bmatrix} 5\times10^{-10} & 0 \\ 0 & 2.5\times10^{-10} \end{bmatrix} \text{m}^2$,	$\theta = 45°$
	Porosity, ε	Mat 1	$\varepsilon_{o,1} = 0.65$	
		Mat 2	$\varepsilon_{o,2} = 0.4$	
		Mat 3	$\varepsilon_{o,3} = 0.5$	
Resin	Viscosity, μ		$\mu_o = 0.7\ \text{Pa}\cdot\text{s}$	

θ: Rotation angle of reinforcement between the principal direction and the Cartesian coordinate system.

4. Verification and Discussion

As already mentioned, the suggested similarity model can predict mold filling of fully three-dimensional geometries. Numerical simulations for locally two-dimensional shell structures, however, were performed to simplify the verification. The part shape, the generated mesh and the elements are shown in Fig. 5. The node and element numbers in the original case are 513 and 936, respectively. The same node and element numbers are used in the sample case. The dimensions of the original shell structure are $0.3 \times 0.2 \times 0.08\ \text{m}^3$ and the thickness of the part is 0.003 m. The sample part is magnified by a scale factor $a_L = 2$ with respect to the original. Three different preforms were used and the resin was sequentially injected through two gates. Material properties used in the original case are given in Table 2 and the injection pressure in the original is defined as

$$P_o(t) = \begin{bmatrix} P_{o,1}(t) = 1\times10^5\ \text{Pa} \\ P_{o,2}(t) = \begin{cases} 0 & 0 \leqslant t < 30 \\ 1.5\times10^5\ \text{Pa} & t \geqslant 30. \end{cases} \end{bmatrix} \tag{28}$$

The scale factors applied in the transformation from the original to the sample case are

$$a_\varepsilon = 0.25, \qquad a_K = 0.5, \qquad a_L = 2. \tag{29}$$

The viscosity in the sample case is

$$\mu_s(t) = 0.7\exp\left[\frac{40}{T_s(t) + 273.15} + 0.01t\right]\text{Pa}\cdot\text{s}, \tag{30}$$

$$\text{where } T_s(t) = \begin{bmatrix} 20 + 0.5t\ °\text{C} & 0 \leqslant t \leqslant 100 \\ 70\ °\text{C} & t \geqslant 100. \end{bmatrix} \tag{31}$$

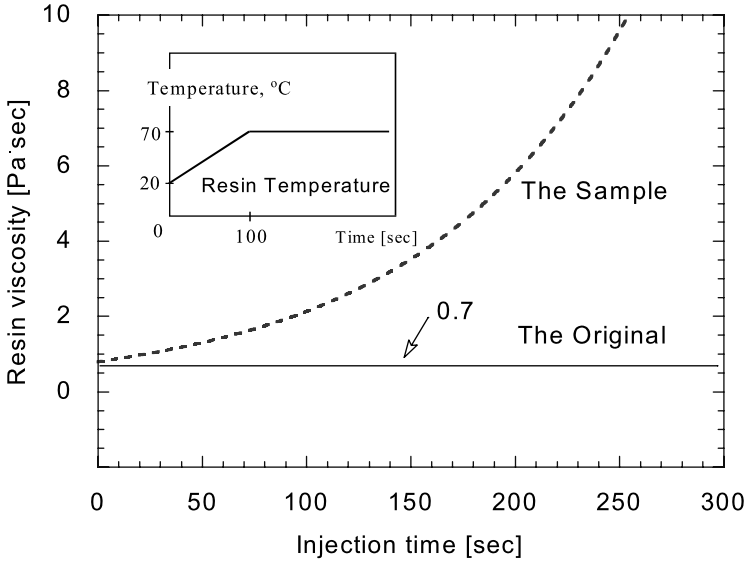

Figure 6. Viscosity variation in the original and sample cases.

The entire quantity of resin has to be premixed before injection and both the resin in the reservoir and that in the mold experience the same temperature history. In general, the viscosity change due to chemical reaction is expressed as a function of temperature and degree of cure [25–28]. For the given cure cycle, however, the viscosity model with temperature and time as variables can be simplified when complete mold filling occurs at an early stage of reaction and the progression of chemical reaction is quite low (equation (30)). If a temperature history of injected resin changes, the coefficients of (30) change. A graphical description of viscosity variation in the original and sample cases is given in Fig. 6. As the verification is performed for multiple gates, equation (8) should be satisfied for the existence of similarity and the ratio of first gate pressures at a specific instant is defined as

$$\frac{P_{s,1}(t)}{P_{o,1}(t)} = 3\sqrt{0.02t + 0.1}. \tag{32}$$

To determine the injection time of the second gate, the time scale transformation is necessary (equation (19)) and the result is given in Fig. 7. The injection time, 56 s in (33) was determined from Fig. 7. The gate pressures for the sample case are

$$P_s(t) = \begin{bmatrix} P_{s,1}(t) = P_{o,1}(t) \times 3\sqrt{0.02t + 0.1}\ \text{Pa} \\ P_{s,2}(t) = \begin{cases} 0 & 0 \leqslant t < 56 \\ P_{o,2}(t) \times 3\sqrt{0.02t + 0.1}\ \text{Pa} & t \geqslant 56. \end{cases} \end{bmatrix} \tag{33}$$

The injection pressures at the two gates of the original and sample cases are shown in Fig. 8.

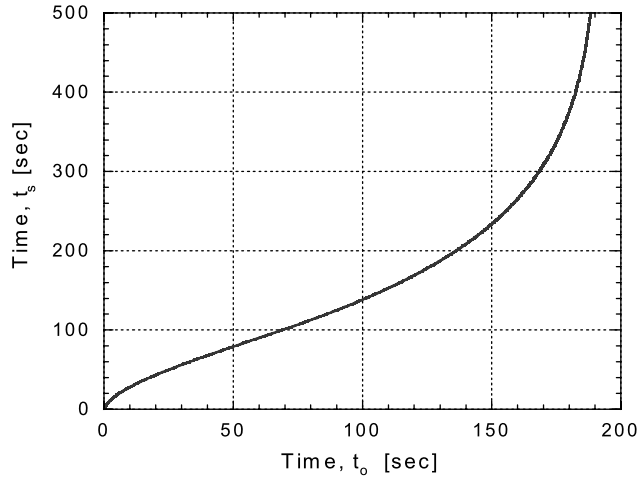

Figure 7. Time scale transformation between the original and the sample.

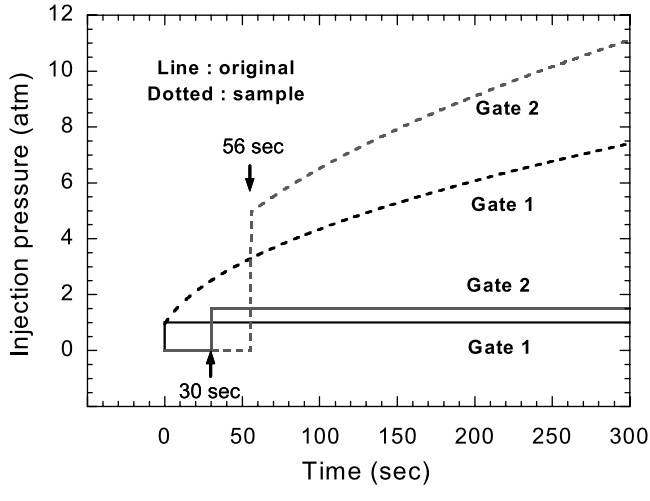

Figure 8. Injection pressures in the original and sample cases.

Using all the properties and conditions defined above, numerical simulations were performed and compared with model predictions. The complete fill times of the original and sample problems were 141.4 s and 211.9 s, respectively. The fill time predicted by the model is 211.6 s and corresponds to an error of about 0.14%. The flow fronts, when matched by the time transformation rule (Fig. 7), are in good agreement as shown in Figs 9 and 10. The pressure fields for the original case at 84.1 s nearly coincide with those of the sample case at 117.6 s (Figs 11 and 12, equation (34)). The velocity fields at 67.9 s for the original case agree well with those at 99.5 s for the sample case, although the agreement is not as good as for the flow fronts and pressure fields (Figs 13 and 14, equation (35)). The slightly in-

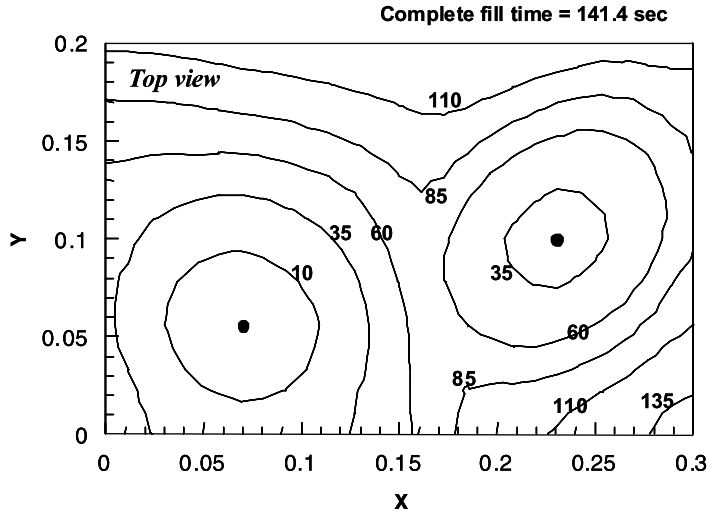

Figure 9. Numerical result of flow front propagations in the original case.

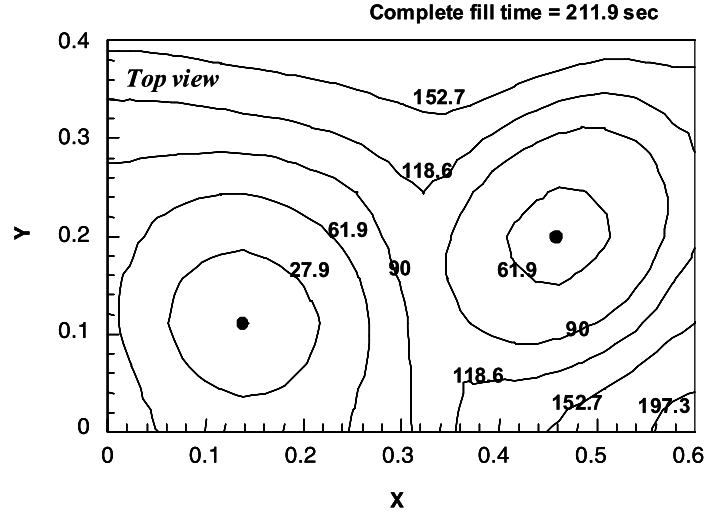

Figure 10. Numerical result of flow front propagations in the sample case.

creased error does not come from the model, but originates in the numerical scheme used in the study.

$$P_{\mathrm{sol},j}(\mathbf{X}_{\mathrm{s},j}, 117.6) = 4.6976 \times P_{\mathrm{sol},j}(\mathbf{X}_{\mathrm{o},j}, 84.1) \quad 1 \leqslant j \leqslant 3, \tag{34}$$

$$\bar{u}_{\mathrm{p}}(\mathbf{X}_{\mathrm{s},j}, 99.5) = 1.8088 \times \bar{u}_{\mathrm{p}}(\mathbf{X}_{\mathrm{o},j}, 67.9) \quad 1 \leqslant j \leqslant 3. \tag{35}$$

The smoothness of the loci lines in Figs 9–14 can be improved by increasing the number of elements in the simulation. The above results prove the validity of the similarity model.

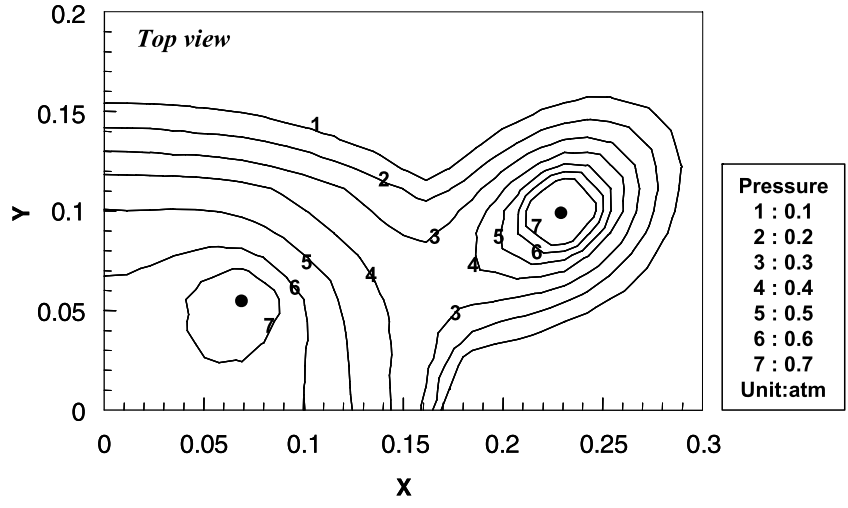

Figure 11. Numerical result of pressure field at the fill time 84.1 s in the original case.

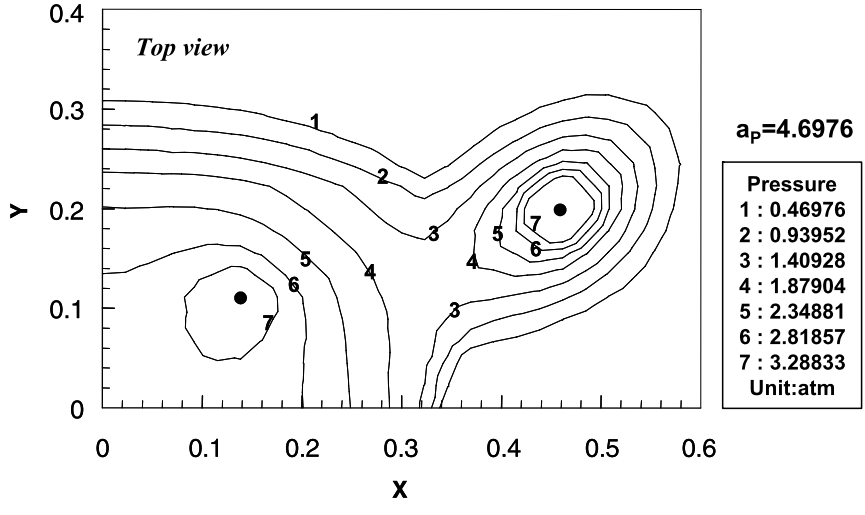

Figure 12. Numerical result of pressure field at the fill time 117.6 s in the sample case.

5. Conclusions

A new method, the similarity technique, was proposed to predict the resin flow in cases with different material, geometric and process parameters in resin transfer molding applications based on only one numerical simulation of a reference case. The existence of similarity solutions was deduced from the linearity and homogeneity of the governing partial differential equation. This yields the similarity relations between various cases where the reinforcement properties (permeability and porosity), the resin property (viscosity), the part dimensions and the injection conditions vary. A control volume based finite element method (CVFEM) was incorporated

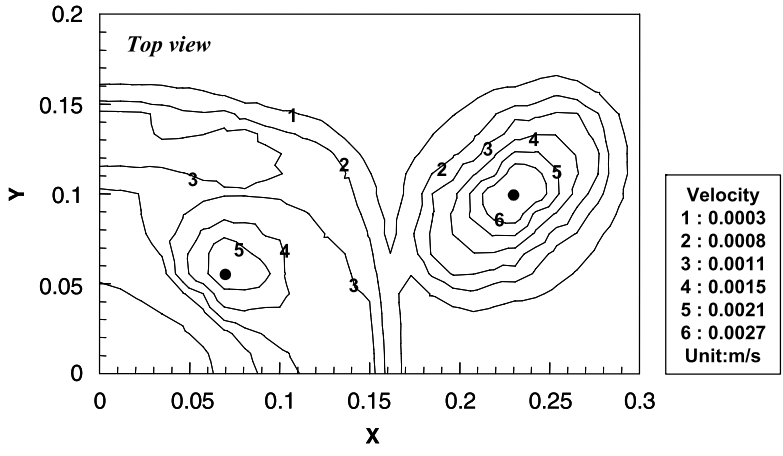

Figure 13. Numerical result of velocity field at the fill time 67.9 s in the original case.

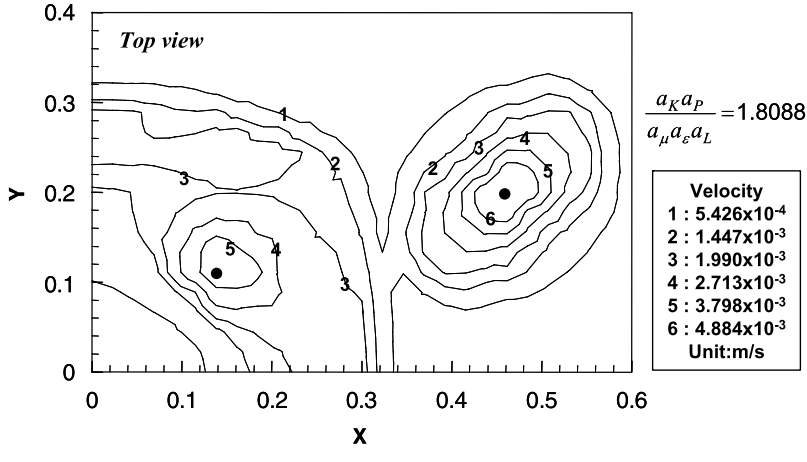

Figure 14. Numerical result of velocity field at the fill time 99.5 s in the sample case.

in the calculation of pressure fields, resin velocity and flow front propagation for a given geometry and injection conditions.

The proposed similarity method was verified by matching the numerical results with those predicted by the similarity model. They show good agreement. The result is an appreciable saving in time and effort, by obviating the need for repeated numerical simulations every time the process parameters change. Furthermore, the similarity model is also very useful in optimizing mold filling conditions.

Acknowledgements

This study has been supported by the KARI under KHP Dual-Use Component Development Program funded by the MKE, and also supported by GRL (Global Research Lab) Program funded by the MEST.

References

1. D. R. Nielsen and R. Pitchumani, Closed-loop flow control in resin transfer molding using real-time numerical process simulations, *Compos. Sci. Technol.* **62**, 283–298 (2002).
2. E. Ruiz, V. Achim, S. Soukane, F. Trochu and J. Bréard, Optimization of injection flow rate to minimize micro/macro-voids formation in resin transfer molded composites, *Compos. Sci. Technol.* **66**, 475–486 (2006).
3. D. Bender, J. Schuster and D. Heider, Flow rate control during vacuum-assisted resin transfer molding (VARTM) processing, *Compos. Sci. Technol.* **66**, 2265–2271 (2006).
4. R. J. Johnson and R. Pitchumani, Flow control using localized induction heating in a VARTM process, *Compos. Sci. Technol.* **67**, 669–684 (2007).
5. Z. Cai, Simplified mold filling simulation in resin transfer molding, *J. Compos. Mater.* **26**, 2606–2630 (1992).
6. A. Boccard, W. I. Lee and G. S. Springer, Model for determining the vent locations and the fill time of resin transfer molds, *J. Compos. Mater.* **29**, 306–333 (1995).
7. J. P. Coulter, B. F. Smith and S. I. Guceri, Experimental and numerical analysis of resin impregnation during the manufacturing of composite materials, in: *Proc. Amer. Soc. Compos. 2nd Tech. Conf.*, pp. 209–217 (1988).
8. F. Trochu and R. Gauvin, Limitations of a boundary fitted finite difference method for the simulation of the resin transfer molding process, *J. Reinf. Plast. Compos.* **11**, 772–786 (1992).
9. M. K. Um and W. I. Lee, A study on the mold filing process in resin transfer molding, *Polym. Engng Sci.* **31**, 765–771 (1991).
10. Y. E. Yoo and W. I. Lee, Numerical simulation of the resin transfer mold filling process using the boundary element method, *Polym. Compos.* **17**, 368–374 (1996).
11. W. B. Young, Resin flow analysis in the consolidation of multi-directional laminated composites, *Polym. Compos.* **16**, 250–257 (1995).
12. B. Liu, S. Bickerton and S. G. Advani, Modeling and simulation of resin transfer molding (RTM) — Gate control, venting and dry spot prediction, *Composites Part A* **27A**, 135–141 (1996).
13. K. M. Pillai and S. G. Advani, Numerical simulation of unsaturated flow in woven fiber preforms during the resin transfer molding process, *Polym. Compos.* **19**, 71–80 (1998).
14. X. Sun, S. Li and L. J. Lee, Mold filling analysis in vacuum-assisted resin transfer molding. Part I: SCRIMP based on a high-permeable medium, *Polym. Compos.* **19**, 807–816 (1998).
15. R. Gauvin and F. Trochu, Key issues in numerical simulation for liquid composite molding processes, *Polym. Compos.* **19**, 233–240 (1998).
16. M. K. Kang and W. I. Lee, A flow front refinement technique for the numerical simulation of the resin-transfer molding process, *Compos. Sci. Technol.* **59**, 1663–1674 (1999).
17. S. T. Lim and W. I. Lee, An analysis of the three-dimensional resin-transfer mold filling process, *Compos. Sci. Technol.* **60**, 961–975 (2000).
18. A. Shojaei, S. R. Ghaffarian and S. M. H. Karimian, Simulation of the three-dimensional non-isothermal mold filling process in resin transfer molding, *Compos. Sci. Technol.* **63**, 1931–1948 (2003).
19. R. Chen, C. Dong, Z. Liang, C. Chang and B. Wang, Flow modeling and simulation for vacuum assisted resin transfer molding process with the equivalent permeability method, *Polym. Compos.* **25**, 146–164 (2004).
20. L. Joubaud, V. Achim and F. Trochu, Numerical simulation of resin infusion and reinforcement consolidation under flexible cover, *Polym. Compos.* **26**, 417–427 (2005).
21. A. Shojaei, A numerical study of filling process through multilayer preforms in resin injection/compression molding, *Compos. Sci. Technol.* **66**, 1546–1557 (2006).

22. C.-Y. Chang, Numerical simulation of the pressure infiltration of fibrous preforms during MMC processing, *Adv. Compos. Mater.* **15**, 287–300 (2006).
23. M. Kaviany, *Principles of Heat Transfer in Porous Media*. Springer-Verlag, Germany (1991).
24. E. B. Becker, G. F. Carey and J. T. Oden, *Finite Elements — An Introduction*. Prentice-Hall, UK (1981).
25. M. R. Dusi, W. I. Lee, P. R. Ciriscioli and G. S. Springer, Cure kinetics and viscosity of Fiberite 976 resin, *J. Compos. Mater.* **27**, 243–261 (1987).
26. D. Rouison, M. Sain and M. Couturier, Resin transfer molding of natural fiber reinforced composites: cure simulation, *Compos. Sci. Technol.* **64**, 629–644 (2004).
27. M. Henne, C. Breyer, M. Niedermeier and P. Ermanni, A new kinetic and viscosity model for liquid composite molding simulations in an industrial environment, *Polym. Compos.* **25**, 255–269 (2004).
28. X. A. Aduriz, C. Lupi, N. Boyard, J.-L. Bailleul, D. Leduc, V. Sobotka, N. Lefèvre, X. Chapeleau, C. Boisrobert and D. Delaunay, Quantitative control of RTM6 epoxy resin polymerisation by optical index determination, *Compos. Sci. Technol.* **67**, 3196–3201 (2007).